

Extended Variational Approach to the $SU(2)$ Mass Gap on the Lattice.

J. O. Akeyo

Physics Department

Kenyatta University

P.O. Box 43844

Nairobi, Kenya

H. F. Jones and C. S. Parker

Physics Department,

Imperial College,

London SW7 2BZ, UK

Abstract

The linear delta expansion is applied to a calculation of the $SU(2)$ mass gap on the lattice. Our results compare favourably with the strong-coupling expansion and are in good agreement with recent Monte Carlo estimates.

1. Introduction

The linear delta expansion (LDE) is an analytic approach to field theory which has been applied to a number of different problems (see for example Ref. [1]). The approach is non-perturbative in the sense that a power series expansion is made in a parameter δ artificially inserted into the action, rather than in a coupling constant of the theory. The calculational techniques required do not differ greatly from conventional Feynman diagrams. An essential part of the approach is an optimization with respect to another parameter, in the present case J , appearing in the δ -extended action.

The linear delta expansion uses δ as an interpolation between a soluble action S_0 and the action for the desired theory S . The action is written:

$$S_\delta = (1 - \delta)S_0 + \delta S, \tag{1}$$

where S_0 contains some dependence on the optimization parameter J . A vacuum generating functional or appropriate Green function may then be evaluated as a power series in δ , which is set equal to unity at the end of the calculation.

Of course this power series is only calculated to a finite number of terms, and will therefore retain some dependence on J which would be absent in the sum to all orders when δ is set equal to one. A well-motivated criterion for fixing J is to demand that, at least locally, the truncated result should be independent of J . This is the principle of minimal sensitivity (PMS) [2]. If C_N denotes the N th approximant to a quantity C , the requirement is

$$\frac{\partial C_N(J)}{\partial J} = 0 \tag{2}$$

This, or some similar criterion, is an intrinsic part of the LDE, providing the non-perturbative dependence on the coupling constant of the theory. For example, in the delta expansion of the integral $\int dx \exp(-gx^4)$, the PMS correctly reproduces its $g^{-1/4}$ dependence. The application of the PMS is also vital for the convergence of the δ series, which

has been rigorously proved for the zero-dimensional ϕ^4 vacuum generating functional [3] and the finite temperature partition function of the anharmonic oscillator in quantum mechanics [4]. The proof has been recently extended [5] to the connected vacuum generating function $W = \ln Z$ in zero dimensions.

A number of non-perturbative approaches to field theory are related to the LDE. At first order in δ , the LDE is related to the Gaussian approximation [6], and at higher orders to generalizations of this [7]. It also has much in common with work of Kleinert [8] and of Sissakian et al. [9].

In the context of lattice gauge theories the LDE has been applied, with various choices of the trial action [10]-[12], to the groups Z_2 , $U(1)$ and $SU(2)$, mainly in calculating the plaquette energy E_P . A particularly useful trial action is the one proposed by Zheng et al. [13], based on single links:

$$S_0 = J \sum_{\ell} \text{tr} U_{\ell} \quad (3)$$

The sum runs over all links ℓ of the lattice, and the parameter J is used for optimization. However, these authors used a different optimization criterion, more closely related to the conventional variational method, in which a rigorous inequality for the free energy at $O(\delta)$ was applied at *all orders in δ* . Such a procedure is liable to forfeit the convergence which may be provided by an order-by-order optimization.

Two of the present authors [14] used the Zheng trial action with the PMS in its usual sense in a calculation of the $SU(2)$ plaquette energy. This was found to give excellent agreement at $O(\delta^3)$ with Monte Carlo results in the weak coupling regime. Following on from this, the phase structure of the mixed $SU(2)$ - $SO(3)$ action was studied [15], and again the results to $O(\delta^3)$ gave good agreement with the Monte Carlo results.

We were therefore encouraged to attempt to extend the method to the more difficult problem of the mass gap in lattice $SU(2)$ using the same trial action. For such quantities, which involve finding the exponential fall-off of a correlator at large separations, semi-

analytic methods have, in principle, an advantage over Monte-Carlo methods, insofar as the size of the lattice is not limited and small signals are not masked by statistics.

In Section 2 we set up the formalism for the problem to be studied and explain how the diagrams which arise in the delta expansion of the modified action are evaluated. The optimization procedure adopted is explained in Section 3, where the results are presented first in lattice units, and then in terms of the SU(2) lattice constant Λ_L by looking for the correct scaling limit as $a \rightarrow 0$. In Section 4 we summarize the paper and indicate some directions for further development. The appendix shows how the evaluation of expectation values in the background of the trial action of Eq. (3) can be organized in a way amenable to symbolic computation.

2. The Diagrammatic Expansion

We consider the $SU(2)$ gauge theory on the lattice. The δ -extended action is :

$$S_\delta = \frac{1}{2}\delta\beta \sum_P \text{tr} U_P + (1 - \delta)J \sum_\ell \text{tr} U_\ell \quad (4)$$

The partition function for this system may be written:

$$\begin{aligned} Z_\delta &= \int [dU] e^{S_\delta} \\ &= \int [dU] \sum_{r=0}^{\infty} \delta^r \frac{(S - S_0)^r}{r!} e^{S_0} \end{aligned} \quad (5)$$

and lattice quantities may be evaluated as power series in δ in the background S_0 . This leads to a diagrammatic expansion related, but not identical to the conventional strong coupling β expansion [16] [17], the difference being that the strong coupling expectations are evaluated in a zero background. The actual diagrams used are also different, the first non-vanishing diagram in the strong coupling expansion for the mass gap being a closed cuboid of plaquettes, compared with the LDE, for which the first diagram is shown in Fig. 1(a).

Calculation of the mass gap involves the evaluation of the connected correlation $C(t)$ between two non-oriented plaquettes A and B with temporal separation ta in any spatial position.

$$C(t) = \langle \text{tr} U_B(ta) \text{tr} U_A(0) \rangle_C \quad (6)$$

The subscript C denotes the connected expectation or cumulant. The diagrammatic expansion in powers of δ has its first non-vanishing term at $O(\delta^t)$. This is shown in Fig. 1(a), where a “ladder” of time-like plaquettes connects A and B .

The next power in δ adds one extra plaquette to Fig. 1(a) in all possible positions. Some examples of these are shown as Figs. 1(b)-(k). It should be noted that this calculation is carried out in the temporal gauge. This explains the absence of diagrams where a plaquette

is attached to the side of the ladder by a temporal link only. Such a link variable is set to unity, and therefore the extra plaquette is effectively disconnected.

At this order, there is also a term proportional to $S^t S_0$ in the δ expansion. This can be included as a partial derivative with respect to J of the $O(\delta^t)$ diagram.

Each of the diagrams shown has an associated multiplicity depending on its geometric properties. The basic diagram of Fig. 1(a) has a factor of $4R_1$ representing the fact that the ladder may be connected to any of the four sides of the lower plaquette A , which is taken as fixed, and that the upper plaquette B has R_1 possible spatial orientations. Similarly the additional factor of $12R_2$ in Fig. 1(b) arises from the R_2 possible spatial orientations of the extra plaquette, its possible attachment on any of the three sides of its neighbour, the fact that either of the two upper plaquettes could be B , and finally a factor of two to include the symmetrical configuration where the extra plaquette is attached to A instead. Note that Figs. 1(f), (h) and (k), which involve an additional plaquette in the body of the ladder, have a t -dependent multiplicity.

Having enumerated the diagrams to the required order and calculated their associated multiplicities, their expectation values must be evaluated. The evaluation of simpler diagrams consisting of up to four or five plaquettes by group integration [13] or character expansion [15] has been discussed elsewhere. Another method is discussed in the appendix to the present paper.

In the evaluation of the straight ladder diagram of Fig. 1(a) and subsequent modifications thereof, an enormous simplification arises from the fact that the expectation value of a single link is a multiple of the identity (Eq. (A1)). This means that the contribution of Fig. 1(a) is just a product of factors representing the expectation values of the doubled links occurring on each rung. Remarkably this factorization extends to the connected expectation value, with the result that

$$C_{1(a)} = (4R_1) 2V_2^6 V^{t+1} \delta^t \quad (7)$$

Here each factor of V_2 represents the expectation value of a single spacelike link of A and B , and we get a factor of $V \equiv \partial V_2 / \partial J$ for each rung. The functions V_n are defined as ratios of modified Bessel functions of argument $2J$:

$$V_n(J) = \frac{I_n(2J)}{I_1(2J)} \quad (8)$$

Two derived quantities which appear frequently in the contributions of higher order diagrams are V as defined above:

$$V(J) = \frac{\partial V_2}{\partial J} \quad (9)$$

and

$$Y(J) = 4V_4 - 6V_3 + 2V_2 \quad (10)$$

The higher order diagrams consist of modifications to this basic diagram by inserting additional plaquettes at either end and/or in the middle. At order δ^{t+1} only one of these alternatives is possible. The factorization property noted above extends to these higher order diagrams. That is, their connected expectation can be obtained from the basic building blocks shown in Fig. 2, with additional factors representing the bulk of the ladder.

Diagrams which involve a modification at one end have a multiplicity which is independent of the total temporal separation t , whereas the three diagrams 1(f), 1(h) and 1(k) which involve an addition to the middle of the ladder have t -dependent multiplicities. The latter essentially exponentiate in higher orders and so are the only ones which contribute to the mass gap when this is calculated from the δ -expansion of the ratio $C(t+1)/C(t)$ (See Eq. (16)). The contributions of these diagrams are given below:

$$\begin{aligned} C_{1(f)} &= (12R_1^2(t-1)) V^{t+2} V_2^8 \delta^{t+1} \\ C_{1(h)} &= (4R_1^2(t-1)) V^t V_2^9 (Y - 8V_2 V) \delta^{t+1} \\ C_{1(k)} &= (2R_1 t) V^{t-1} V_2^6 (Y^2/3 - 16V_2^2 V^2) \delta^{t+1} \end{aligned} \quad (11)$$

The diagrams of order δ^{t+2} are similarly built up by adding a further plaquette in all possible ways. Some examples are shown in Fig. 3. There are around 150 diagrams at this order, although again it is only those with t -dependent multiplicities which contribute to the δ -expansion of $C(t+1)/C(t)$. There are also additional terms in $S^t S_0^2$ and $S^{t+1} S_0$ which arise from the expansion of the factor $(S - S_0)^r$ in Eq. 5. The most succinct way of including such contributions is to note that J always occurs in the combination $J(1 - \delta)$ (See Eq. (4)). Thus the V 's occurring in the various expectation values are really functions of this argument, which needs to be Taylor expanded to the appropriate order. Altogether we may write

$$C(t) = \sum_i M_i D_i(J(1 - \delta)) \tag{12}$$

where M_i denotes the multiplicity of the i th diagram and D_i is its connected expectation value.

3. Extraction of the mass gap

Having set up the diagrams necessary to calculate the correlation $C(t)$, we now need to extract the mass gap m using the familiar result:

$$C(t) \sim A e^{-mat} \quad (13)$$

as $t \rightarrow \infty$, giving

$$ma = \lim_{t \rightarrow \infty} \ln \frac{C(t)}{C(t+1)} \quad (14)$$

At first sight it might seem reasonable to calculate $C(t)$ and $C(t+1)$ separately, applying the PMS to each correlation, and then to extract ma from equation (14). However, this is not a fruitful procedure for two reasons. The first is that it is not in the spirit of the PMS, according to which it is the final quantity calculated which should be optimized with respect to J . More importantly, the convergence of the expansion performed in this manner is extremely slow. It is, after all, asking a great deal of a perturbation expansion, even when optimized, to give the correct $t \rightarrow \infty$ limit of $C(t)$ with only a few terms of the expansion.

The most important aspect of the problem is that some of the diagrams have multiplicities which grow with t , reflecting the fact that additional plaquettes can be attached in a large number of positions to the body of the ladder. Thus the larger the value of t , the higher the order of the perturbation expansion required before the factorial denominators in Eq. (5) eventually control the convergence. However, these diagrams essentially exponentiate. For example the series of “bracket” diagrams starting with Fig. 1(h) and continuing with Fig. 3(h) has the form of an exponential series for large t . Consequently, when the series for the *ratio* is taken the t -dependence cancels, as we show in more detail below. Thus by considering the Taylor expansion for the ratio, the limit $t \rightarrow \infty$ does not pose such a threat to the convergence of the series. A similar procedure was adopted by

Münster [17] in the application of the strong coupling expansion to the calculation of the mass gap.

We therefore apply the PMS to the Taylor expansion of the ratio $C(t+1)/C(t)$, up to third order in δ . Writing the series for $C(t)$ and $C(t+1)$ as

$$\begin{aligned} C(t) &= \delta^t(b_0 + b_1\delta + b_2\delta^2 + \dots) \\ C(t+1) &= \delta^{t+1}(a_0 + a_1\delta + a_2\delta^2 + \dots), \end{aligned} \quad (15)$$

the ratio has the expansion

$$\frac{C(t+1)}{C(t)} = \frac{a_0}{b_0}\delta + \frac{a_1b_0 - a_0b_1}{b_0^2}\delta^2 + \frac{b_1(a_0b_1 - a_1b_0) - b_0(a_0b_2 - a_2b_0)}{b_0^3}\delta^3 + \dots \quad (16)$$

This formulation leads to a naïve large t limit for the mass gap. In going from temporal separation t to $t+1$, we add an extra plaquette to the ladder part of each diagram, which gives an overall extra factor $\frac{1}{2}\beta V(J)$ to the correlation. Thus one might expect the mass gap to be equal to $-\ln(\frac{1}{2}\beta V(J))$. In fact, for the lowest-order contribution we have

$$\begin{aligned} a_0 &= f_0\lambda^{t+1} \\ b_0 &= f_0\lambda^t \end{aligned} \quad (17)$$

where $\lambda = \frac{1}{2}\beta V$, so that indeed $a_0/b_0 = \frac{1}{2}\beta V$. In higher orders, however, t -dependent multiplicities give rise to corrections to the naïve result.

The next-order coefficients have the form:

$$\begin{aligned} a_1 &= (f_1 + (t+1)g_1)\lambda^{t+1} \\ b_1 &= (f_1 + tg_1)\lambda^t \end{aligned} \quad (18)$$

Then to second order in δ , Eq. (16) is:

$$\frac{C(t+1)}{C(t)} = \delta\left[\lambda + \delta\frac{\lambda g_1}{f_0}\right] \quad (19)$$

Again this is independent of t , and means that in this form of the expansion t does not need to be taken asymptotically large. It is sufficient to take it large enough for the diagrams to settle down to a generic form.

At $O(\delta^{t+2})$, writing

$$\begin{aligned} a_2 &= (f_2 + (t+1)g_2 + (t+1)^2h_2)\lambda^{t+1} \\ b_2 &= (f_2 + tg_2 + t^2h_2)\lambda^t, \end{aligned} \tag{20}$$

the $O(\delta^3)$ term in Eq. (16) is:

$$\frac{b_1(a_0b_1 - a_1b_0) - b_0(a_0b_2 - a_2b_0)}{b_0^3} = \frac{\lambda}{f_0^2} [f_0(h_2 + g_2) - f_1g_1 + t(2h_2f_0 - g_1^2)] \tag{21}$$

This apparently has a t -dependence, but in fact the coefficient h_2 is precisely $\frac{1}{2}g_1^2/f_0$ because it arises from exponentiation of the t -dependent graphs at order δ^{t+1} . As emphasized by Münster [17], the summation over the spatial positions of the upper plaquette B , which also serves to project out zero spatial momentum in the correlator, is vital to this exponentiation.

Altogether, then, we have the t -independent result for the ratio to order δ^3 :

$$\frac{C(t+1)}{C(t)} = \delta\lambda \left[1 + \delta\frac{g_1}{f_0} + \frac{\delta^2}{f_0^2}(f_0(h_2 + g_2) - f_1g_1) \right]. \tag{22}$$

This expression for $C(t+1)/C(t)$ is still a function of J . According to the PMS criterion, we are looking for stationary points in J . Typical curves of the J dependence are shown in Figs. 4 and 5 for $O(\delta^{t+1})$ and $O(\delta^{t+2})$ respectively. At $O(\delta^{t+1})$ there is a single maximum, and at $O(\delta^{t+2})$ the value of $C(t+1)/C(t)$ at the maximum is remarkably close to this, even though the position in J is quite different.

At this stage our result is expressed in terms of the inverse of the lattice spacing a , which we need to take to zero in order to make contact with the continuum limit. The physical value of the glueball mass must in this limit become a fixed number times the SU(2) lattice scale Λ_L . In the weak coupling limit, to two-loop level, this is given by

$$\Lambda_L a = \left(\frac{6\pi^2\beta}{11} \right)^{51/121} \exp \left(-\frac{3\pi^2\beta}{11} \right) \quad (23)$$

We look for the constant C_m such that

$$ma = C_m \Lambda_L a, \quad (24)$$

which is the value for which the graph of Eq. (23) against β is tangential to that of ma calculated in the LDE. The graphs are shown in Fig. 6 to $O(\delta^{t+1})$ and Fig. 7 to $O(\delta^{t+2})$. These show good agreement between the orders, the tangents occurring at $\beta = 2.62$ and $\beta = 2.64$ at $O(\delta^{t+1})$ and $O(\delta^{t+2})$ respectively. These results then give for the mass gap:

$$\begin{aligned} m &= 184\Lambda_L & (O(\delta^{t+1})) \\ m &= 197\Lambda_L & (O(\delta^{t+2})) \end{aligned} \quad (25)$$

Compared to the strong-coupling expansion [17], which gives $m = 193\Lambda_L$ ($\beta \approx 2.3$) at order β^6 and $m = 127\Lambda_L$ ($\beta \approx 1.9$) at order β^8 , our results show better consistency between consecutive orders; moreover, the β -values where the tangents occur are further into the weak-coupling region. In a series expansion of this kind it is difficult to quote a precise error, but based on the difference between our two results at $O(\delta^{t+1})$ and $O(\delta^{t+2})$ one would estimate the error as not more than ± 13 .

Our results can be compared directly with those of Berg and Billoire [18], who quote $m = (190 \pm 10)\Lambda_L$. A comparison with the more recent work of Michael and Perantonis [19] on a 32^4 lattice is less straightforward, since they quote their results in lattice units and cast some doubt on the validity of asymptotic scaling. Nonetheless, converting $m = 197\Lambda_L$ to lattice units at $\beta = 2.5$ gives $ma = 0.70$, in excellent agreement with their results. At $\beta = 2.7$ it gives $ma = 0.42$, which is slightly higher than their central value, but still within the error bars.

4. Conclusions

In this paper we have demonstrated that the linear delta expansion with the principle of minimal sensitivity is a viable technique for the calculation of the mass gap for a lattice gauge theory. We have shown how the lattice diagrams appearing in this type of calculation can be easily evaluated by a process of building up chains of plaquettes from a simple ‘root’ diagram, and that connected expectations of these are as simple to deal with. The gauge fixing procedure adopted reduces the number of contributing diagrams, and makes them easier to evaluate.

As always, the PMS is an integral part of the calculation. The potential ambiguity arising from the occurrence of multiple PMS points is not serious in this case. It is clear by comparison with the lower-order calculation that it is the broad maximum at $O(\delta^{t+2})$ which is the appropriate one, and it is very encouraging that the resulting value of m is so stable in going from one order to the next.

This calculation has shown the relationship between the LDE and the strong coupling expansion. The diagrammatic expansion used is similar, but the actual evaluation of the diagrams is different, requiring alternative techniques.

It has proved sufficient to work with the correlators of simple plaquette operators rather than the more complicated “fuzzy” operators which have been found necessary in Monte-Carlo calculations. The fundamental reason for this is that we are effectively working on an infinite lattice, so that large separations are no problem, whereas in Monte-Carlo calculations it is necessary to enhance the signal at finite separations.

The present calculation could be extended in various ways. In increasing order of difficulty these are:

(i) to calculate higher mass glueball states. With a simple plaquette operator the $J^{PC} = 2^{++}$ state occurring in the E^+ representation of the cubic group is accessible by weighting the different orientations of the upper plaquette. Other spin-parities would require larger

Wilson loops.

(ii) to work with the gauge group $SU(3)$ rather than $SU(2)$. This would involve an extension of the techniques of the Appendix to $SU(3)$.

(iii) to go to next order in the δ expansion. The difficulty here is the greatly increased number of diagrams which have to be taken into account and the consequent danger of missing an important contribution.

Further possible extensions include calculations of the string tension and various quantities at finite temperature. Some work has already been done on these lines by Tan and Zheng [20], but using the free energy criterion mentioned above. It would be interesting to return to these problems using PMS optimization order by order in the quantity being calculated.

A Appendix

In this appendix we wish to explain a method for calculating (connected) expectation values of a string of plaquette operators in the background of our trial action S_0 (Eq. (3)). The method involves expressing the expectation values of products of single link operators in terms of tensor projection operators [21], which can then be multiplied together within an algebraic manipulation package. Of those available, we found FORM the most suitable because it has an explicit summation convention and extensive substitution facilities.

Let us start with the simplest example, $\langle U \rangle$, where U is a single-link element of $SU(2)$. It is clear that $\langle U_a^i \rangle \propto (Y_{\square})_a^i := \delta_a^i$, and by taking the trace we establish the coefficient as V_2 (see Eq. (8)):

$$\langle U_a^i \rangle = (V_2 Y_{\square})_a^i \quad (\text{A1})$$

The notation has been chosen with a view to subsequent examples and in general refers to the Young tableau associated with a particular permutation symmetry, in this case trivial, of the upper indices.

For the product of two U 's belonging to the same link, there is similarly no difficulty (again by taking appropriate contractions) in showing that

$$\langle U_a^i U_b^j \rangle = (V_3 Y_{\square\square} + Y_{\square})_{ab}^{ij} \quad (\text{A2})$$

where

$$\begin{aligned} (Y_{\square\square})_{ab}^{ij} &= \frac{1}{2}(\delta_a^i \delta_b^j + \delta_a^j \delta_b^i) \\ (Y_{\square})_{ab}^{ij} &= \frac{1}{2}(\delta_a^i \delta_b^j - \delta_a^j \delta_b^i) \end{aligned} \quad (\text{A3})$$

Here $Y_{\square\square}$ and Y_{\square} are indeed projection operators which correspond to the two irreducible representations of the permutation group of the upper indices relative to the lower ones.

If we now go on to the product of three U 's, there are three irreducible representations of the relevant permutation group S_3 . However, since we are constructing irreducible tensors of $SU(2)$, the completely antisymmetric operator Y_{\square} effectively vanishes and only the completely symmetric and mixed symmetry operators $Y_{\square\square}$ and $Y_{\square\blacksquare}$ survive.

The form of these tensors can be deduced from the group algebra of the conjugacy classes of S_3 , which comprise E , $B := 3C_2$ and $C := 2C_3$. The non-trivial products in the algebra are $B^2 = 3(E + C)$, $BC = CB = 2B$ and $C^2 = 2E + C$. The vanishing of Y_{\square} for $SU(2)$ corresponds to the equivalence relation $B \equiv E + C$ when acting on the identity element $\delta_a^i \delta_b^j \delta_c^k$. Thus in our search for projection operators we can limit ourselves to the sub-algebra of A_3 generated by the even permutations of E , C . It is then easy to construct the required projection operators as

$$\begin{aligned} Y_{\square\square} &= \frac{1}{3}(E + C) \\ Y_{\square\blacksquare} &= \frac{1}{3}(2E - C) \end{aligned} \quad (\text{A4})$$

acting on $\delta_a^i \delta_b^j \delta_c^k$ by permutation of the upper indices. By taking traces we can establish the coefficients as V_4 , V_2 in the expansion

$$\langle U_a^i U_b^j U_c^k \rangle = (V_4 Y_{\square\square} + V_2 Y_{\square\blacksquare}) \delta_a^i \delta_b^j \delta_c^k \quad (\text{A5})$$

For the product of four U 's, we can anticipate that

$$\langle U_a^i U_b^j U_c^k U_d^l \rangle = (V_5 Y_{\square\square\square\square} + V_3 Y_{\square\blacksquare\blacksquare} + Y_{\square\blacksquare\square}) \delta_a^i \delta_b^j \delta_c^k \delta_d^l \quad (\text{A6})$$

The problem is to establish the specific form of the three projection operators. Again the procedure is to look at the group algebra of S_4 , which has five conjugacy classes. Because of the equivalence relations arising from the vanishing in $SU(2)$ of completely antisymmetric combinations involving more than two indices, we can eliminate the classes of odd permutations and work with the group algebra of the alternating group A_4 . This

has three classes, E , $B := 3C_2$, $C := 8C_3$, with algebra $B^2 = 3E + 2B$, $BC = CB = 3B$ and $C^2 = 8E + 8B + 4C$. From these it is possible to construct the projection operators

$$\begin{aligned} Y_{\square\square\square} &= \frac{1}{12}(E + B + C) \\ Y_{\square\square} &= \frac{1}{4}(3E - B) \\ Y_{\square} &= \frac{1}{12}(2(E + B) - C) \end{aligned} \quad (\text{A7})$$

These formulae are sufficient to evaluate all the diagrams we encountered up to $O(\delta^{t+2})$.

Diagrams involving U^\dagger can be dealt with [21] by converting U^\dagger to U according to

$$\begin{aligned} (U^\dagger)_a^i &= \epsilon^{ib} \epsilon_{aj} U_b^j \\ &= (\delta_a^i \delta_j^b - \delta_a^b \delta_j^i) U_b^j \end{aligned} \quad (\text{A8})$$

In particular,

$$\langle U_a^i U_b^{\dagger j} \rangle = \left(\frac{1}{2}(V_3 + 1)Y_{\square} + \frac{1}{2}(3V_3 - 1)Y_{\square} \right)_{ab}^{ij} \quad (\text{A9})$$

A given diagram will consist of a number of plaquettes with certain links in common. The procedure is then to write down the general expression for the corresponding amplitude, identify the shared links, apply the appropriate substitutions for $\langle UU \rangle$, $\langle UU^\dagger \rangle$, $\langle UUU \rangle$ and $\langle UUUU \rangle$ and then sum over all repeated indices.

In fact we actually want the connected expectation values (cumulants) $\langle \rangle_C$. These can be obtained by identifying the different terms in the expansion of $\prod_{i=1}^N (\partial/\partial x_i) \ln Z$ with products of expectation values of the corresponding partitions of the N plaquettes.

Thus

$$\frac{\partial}{\partial x} \frac{\partial}{\partial y} \ln Z = \frac{1}{Z} \frac{\partial^2 Z}{\partial x \partial y} - \left(\frac{1}{Z} \frac{\partial Z}{\partial x} \right) \left(\frac{1}{Z} \frac{\partial Z}{\partial y} \right) \quad (\text{A10})$$

corresponds to

$$\langle UV \rangle_C = \langle UV \rangle - \langle U \rangle \langle V \rangle \quad (\text{A11})$$

etc.

These identifications can all be implemented within a short FORM program.

References

- [1] H. F. Jones in *Proceedings of LP-HEP 91*, p. 111 (World Scientific 1992).
- [2] P. M. Stevenson, *Phys. Rev.* **D23** (1981) 2916.
- [3] I. R. C. Buckley, A. Duncan and H. F. Jones, *Phys. Rev.* **D47** (1993) 2554.
- [4] A. Duncan and H. F. Jones, *Phys. Rev.* **D47** (1993) 2560.
- [5] C. M. Bender, A. Duncan and H. F. Jones, Imperial College Preprint TP/92-93/55, to be published in *Phys. Rev. D*.
- [6] P. M. Stevenson, *Phys. Rev.* **D32** (1985) 1389.
- [7] A. Okopińska, *Phys. Rev.* **D35** (1987) 1835.
- [8] H. Kleinert, *Phys. Lett.* **B280** (1992)251.
- [9] A. N. Sissakian, I. L. Solovtsov and O. P. Solovstova *Phys. Lett.* **B321** (1994) 381.
- [10] A. Duncan and M. Moshe, *Phys. Lett.* **B215** (1988) 352.
- [11] I. R. C. Buckley and H. F. Jones, *Phys. Rev.* **D45** (1992) 654.
- [12] I. R. C. Buckley and H. F. Jones, *Phys. Rev.* **D45** (1992) 2073.
- [13] X. Zheng, Z. G. Tan and J. Wang, *Nucl. Phys.* **B287** (1987) 171.
- [14] J. O. Akeyo and H. F. Jones, *Phys. Rev.* **D47** (1993) 1668.
- [15] J. O. Akeyo and H. F. Jones, *Z. Phys.* **C58** (1993) 629.
- [16] M. Creutz, *Quarks, Gluons and Lattices* (Cambridge University Press, Cambridge, 1983).

- [17] G. Münster, Nucl. Phys. **B190** (1981) 439.
Errata: Nucl. Phys. **B200** (1982) 536, and Nucl. Phys. **B205** (1982) 648.
- [18] B. A. Berg and A. H. Billoire, Phys. Rev. **D40** (1989) 550.
- [19] C. Michael and S. J. Perantonis, J. Phys. **G18** (1992) 1725.
- [20] C-I Tan and X. Zheng, Phys. Rev. **D39** (1989) 623.
- [21] W. Kerler and T. Metz, Phys. Rev. **D44** (1991) 1263.

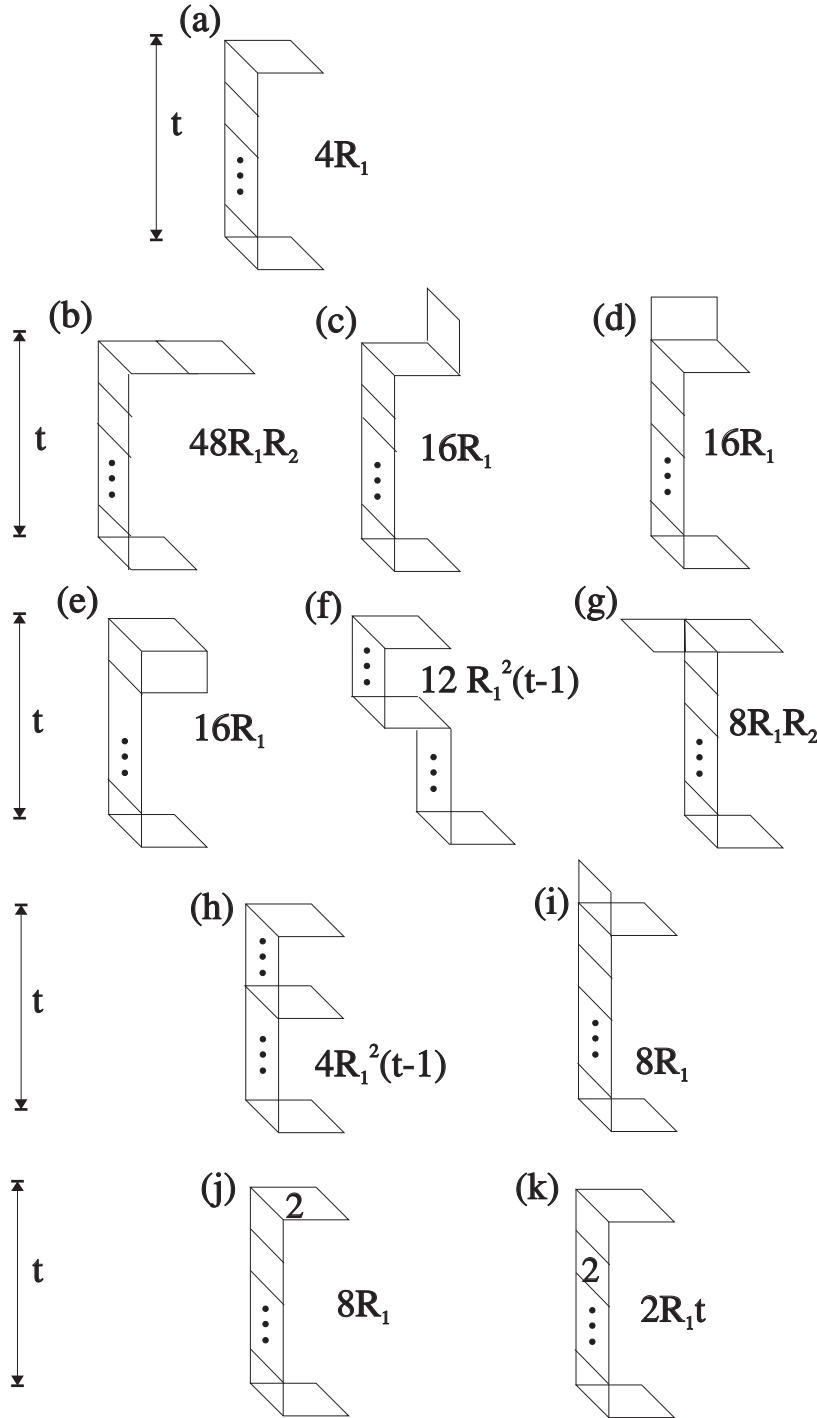


Figure 1: Non-vanishing diagrams at $O(\delta^t)$ and $O(\delta^{t+1})$ in the linear delta expansion for the $SU(2)$ mass gap. The vertical direction represents time. The expression next to each diagram is its geometric multiplicity factor. The R_i are defined by $R_i = 2d - 3 - i$ for d spacetime dimensions.

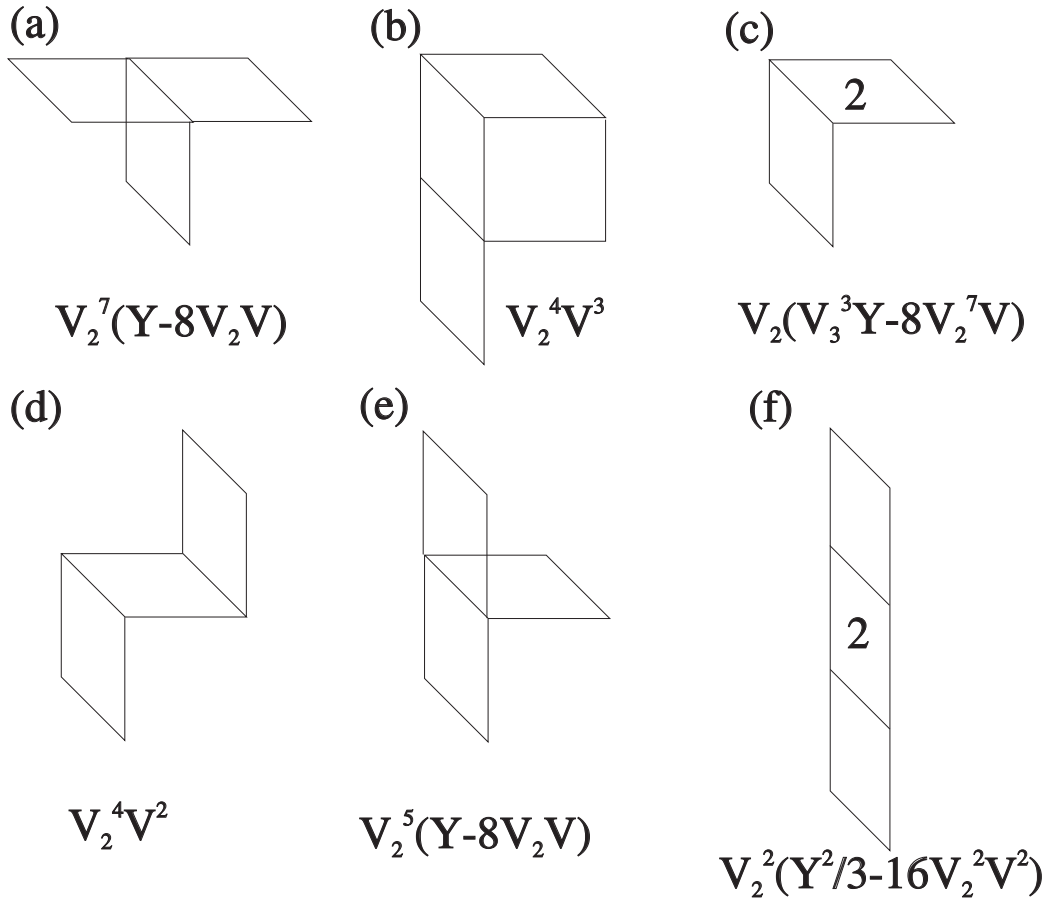


Figure 2: Connected expectations of some of the basic diagrams used in calculating the correlation $C(t)$. The symbols used are defined in the text.

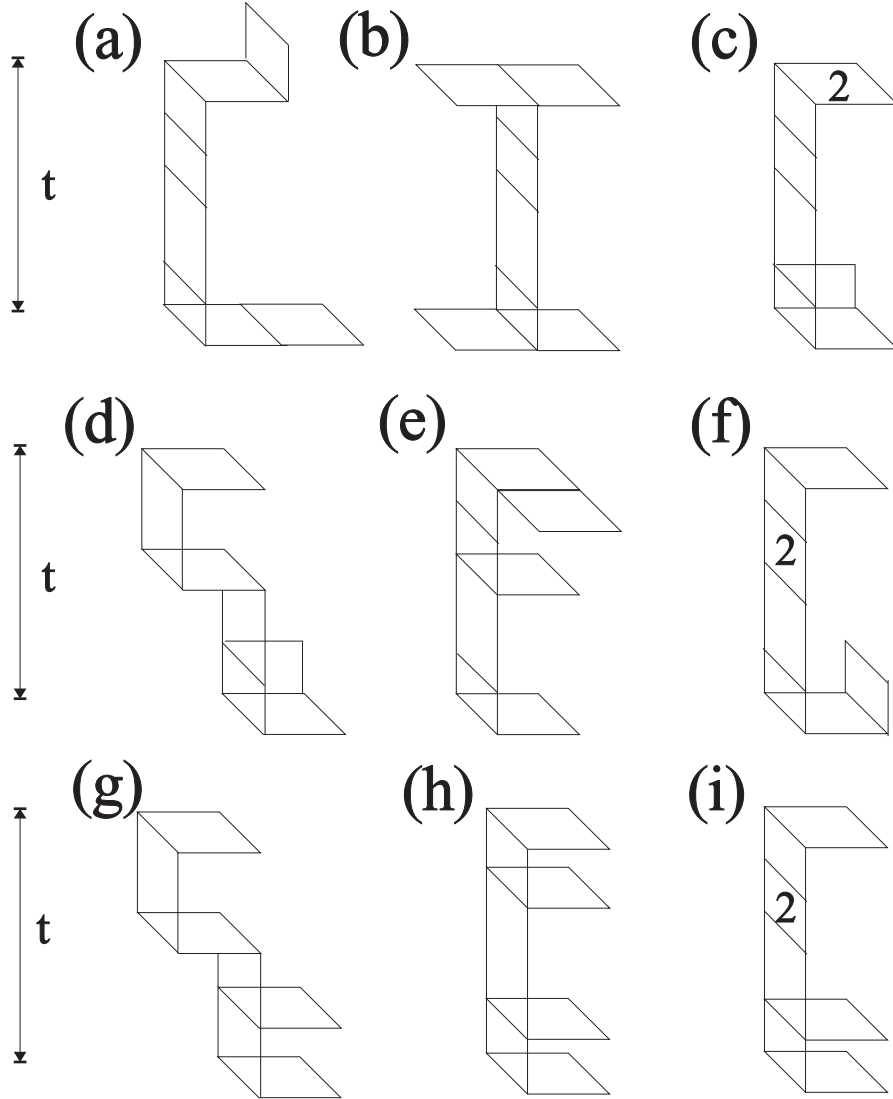


Figure 3: Examples of non-vanishing diagrams at $O(\delta^{t+2})$ in the delta expansion for the $SU(2)$ mass gap. The vertical direction represents time. Diagrams (a)-(c) have multiplicity independent of t , (d)-(f) have multiplicity $\propto t$, and (g)-(i) have multiplicity $\propto t^2$.

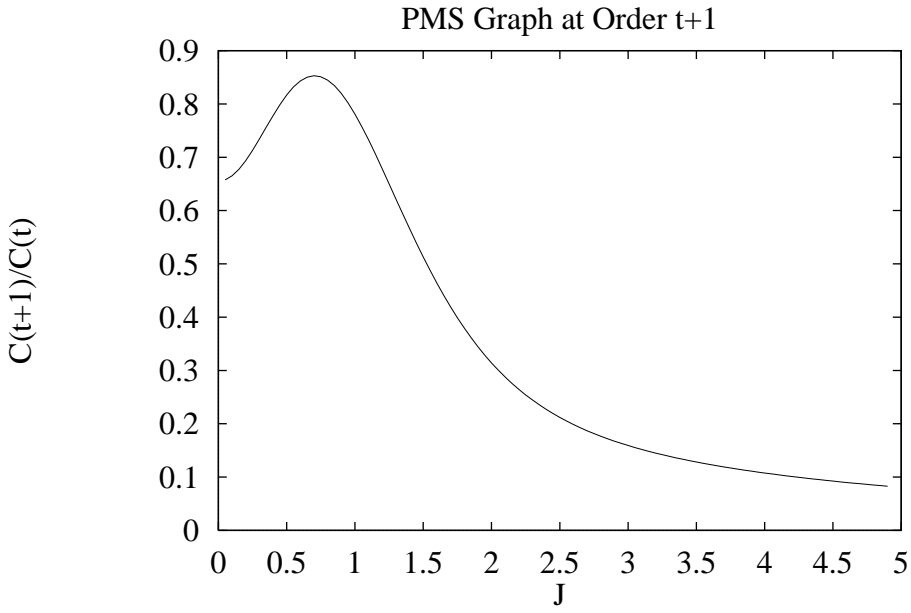


Figure 4: $O(\delta^{t+1})$ PMS graph ($\beta = 2.62$).

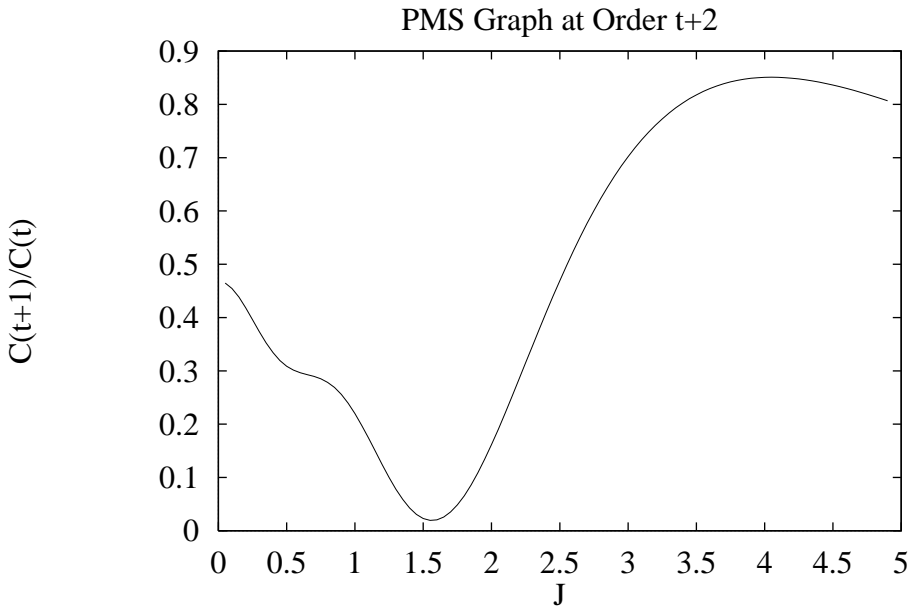


Figure 5: $O(\delta^{t+2})$ PMS graph ($\beta = 2.64$).

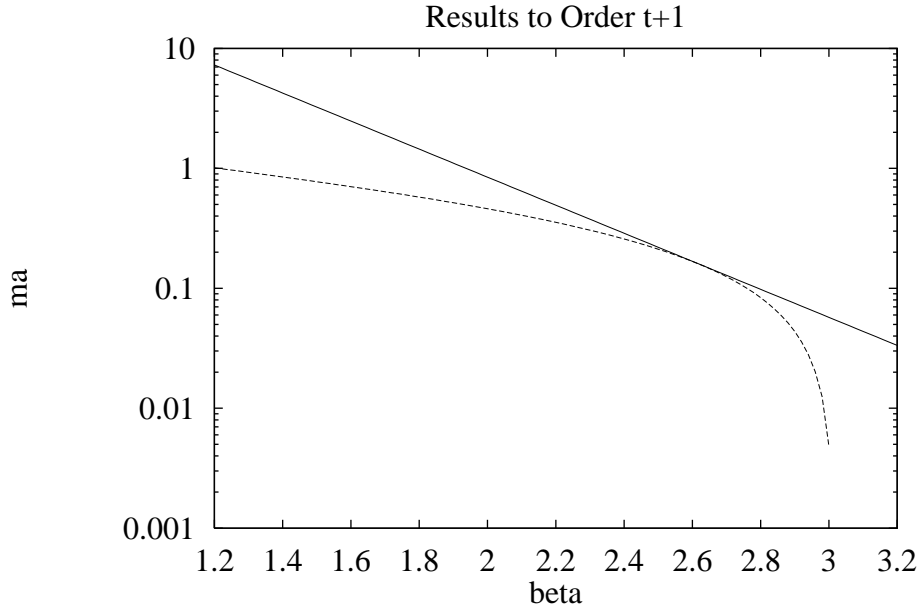


Figure 6: $O(\delta^{t+1})$ results for ma (dotted line), compared with weak coupling renormalization group formula for $\Lambda_L a$ (solid line), with $C_m = 184$.

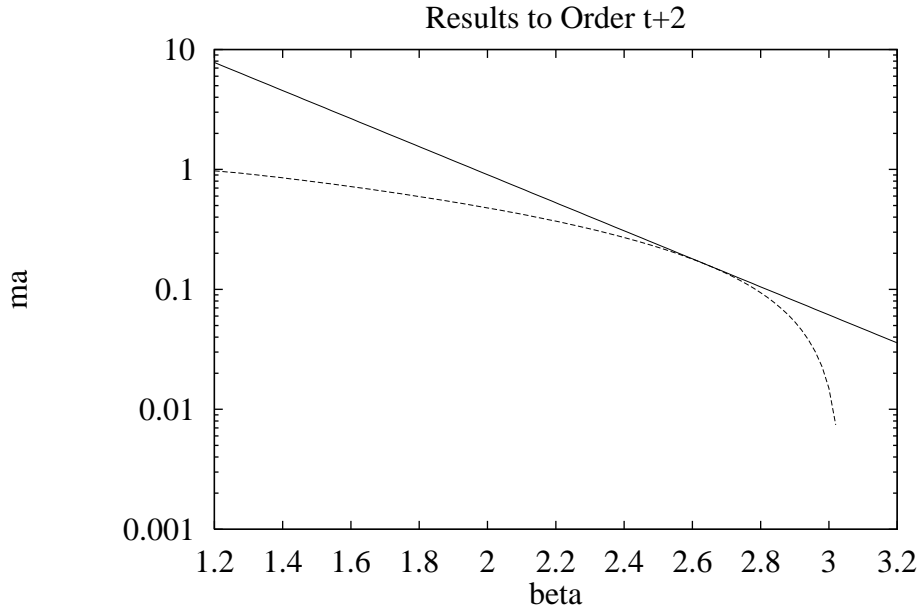


Figure 7: $O(\delta^{t+2})$ results for ma (dotted line), compared with weak coupling renormalization group formula for $\Lambda_L a$ (solid line), with $C_m = 197$.